

Insoluble tau aggregates induce neuronal death through modification of membrane ion conductance, activation of voltage-gated calcium channels and NADPH oxidase

Noemi Esteras¹ , Franziska Kundel², Giuseppe F. Amodeo³, Evgeny V. Pavlov³, David Klenerman² and Andrey Y. Abramov¹ 

¹ Department of Clinical and Movement Neurosciences, UCL Queen Square Institute of Neurology, London, UK

² Department of Chemistry, University of Cambridge, UK

³ Department of Basic Sciences, New York University College of Dentistry, NY, USA

Keywords

BLM; insoluble tau; NADPH oxidase; nifedipine; voltage-gated calcium channels

Correspondence

A. Y. Abramov and N. Esteras, Department of Clinical and Movement Neurosciences, UCL Queen Square Institute of Neurology, Queen Square, London WC1N 3BG, UK
Tel: +44 2078 3736 11
E-mails: a.abramov@ucl.ac.uk (AYA); n.gallego@ucl.ac.uk (NE)

(Received 20 December 2019, revised 12 March 2020, accepted 20 April 2020)

doi:10.1111/febs.15340

Most neurodegenerative disorders are associated with aggregation and accumulation of misfolded proteins. One of these proteins, tau, is involved in a number of pathologies including Alzheimer's disease and frontotemporal dementia. Aggregation and phosphorylation of tau have been shown to be a trigger for abnormal signal transduction and disruption of cellular homeostasis. Here, we have studied the effect of extracellular tau at different stages of aggregation in cortical co-cultures of neurons and astrocytes, to understand how this process affects tau pathogenicity. We found that the species formed after prolonged *in vitro* aggregation of tau (longer than 1 day) are able to stimulate reactive oxygen species (ROS) production through the activation of NADPH oxidase without decreasing the level of the endogenous antioxidant glutathione. The same late insoluble aggregates of tau induced calcium signals in neurons and a gradual increase in the ionic current of artificial membranes. Both tau-induced calcium signals and ROS production in NADPH oxidase were reduced in the presence of the inhibitor of voltage-gated calcium channels (VGCC) nifedipine. This suggests that insoluble aggregates of tau incorporate into the membrane and modify ionic currents, changing plasma membrane potential and activating VGCCs, which induces a calcium influx that triggers ROS production in NADPH oxidase. The combination of all these effects likely leads to toxicity, as only the same insoluble tau aggregates which demonstrated membrane-active properties produced neuronal cell death.

Introduction

Despite the difference in aetiology and in the mechanisms of pathology, most neurodegenerative disorders have similar features such as the accumulation of abnormally aggregated proteins and the involvement of mitochondria and oxidative stress in the pathogenesis.

In Alzheimer's disease (AD), the protein tau becomes abnormally clumped to form 'tangles'. This clumping process is highly dynamic, and during it, a number of intermediates are formed which differ in size, structure and morphology. Abnormal deposition of aggregates of the protein tau is involved in a

Abbreviations

AD, Alzheimer's disease; AEBSF, 2-aminoethyl)benzenesulfonyl fluoride hydrochloride; DHE, dihydroethidium; EGTA, ethyleneglycol-bis(beta-aminoethylether)-*N,N*-tetraacetic acid; ER, endoplasmic reticulum; GSH, reduced glutathione; NOX, NADPH oxidase; ROS, reactive oxygen species; SERCA, sarco/endoplasmic reticulum Ca²⁺ ATPase; ThT, thioflavin T; TIRF, total internal reflection fluorescence microscopy; VGCCs, voltage-gated calcium channels.

number of neurodegenerative diseases (termed tauopathies). This group comprises more than 20 clinicopathological entities, including AD, progressive supranuclear palsy, frontotemporal dementia, Pick's disease, corticobasal degeneration and chronic traumatic encephalopathy. Together, genetic and pathological evidence suggests that the protein tau and its aggregation are central to the pathogenesis of neurodegeneration and dementia in these conditions.

For a long time, it was accepted that intracellular tangles of tau might possibly affect cellular function. However, the identification of prion-like propagation of misfolded proteins, whereby assemblies can be released and spread to neighbouring cells (to seed the aggregation of native monomers initiating the formation of additional aggregates), suggested pathological mechanisms that are not limited to intracellular aggregates.

There are significant gaps in our understanding of tau disease biology, including the toxicity of tau (if any) and if the acquisition of amyloidogenic structures results in toxicity gain and how the function of tau changes with its aggregation state. It is also not very clear which structure of tau is involved in the mechanism of disease.

Some of the characteristics of tauopathies are abnormal signal transduction, including calcium signalling, mitochondrial dysfunction and excessive production of reactive oxygen species (ROS) [1,2].

Oxidative stress has been shown to be one of the major triggers for neurodegeneration. Involvement of misfolded proteins in the generation of free radicals and oxidative stress was shown for a number of neurodegenerative diseases [3,4]. Thus, beta-amyloid produces ROS through activation of NADPH oxidase (NOX) [5,6]; α -synuclein oligomers are able to produce superoxide [7,8]; and endogenous tau is able to induce ROS production and oxidative stress in mitochondria [2].

Calcium signalling controls almost all cellular processes. Alteration of the calcium signal in neurons and astrocytes leads to changes in the signal transduction between cells, calcium overload in mitochondria and induction of the mechanism of cell death. Importantly, oligomerization of misfolded proteins makes them able to modify the cellular membranes leading to the induction of calcium signals [9]. Initially, this was shown for beta-amyloid [10–12] and later for α -synuclein [13,14]. The ability of tau to produce ion channels in artificial membranes has also been previously shown [15–17]. However, very little is known about the role of tau and its aggregates in redox homeostasis and calcium signalling compared to other misfolded proteins.

Recently, the kinetic parameters of the assembly and replication of aggregates of full-length recombinant tau were determined, showing that tau aggregates have an intrinsic ability to amplify by filament fragmentation [18]. Here, we have studied the toxicity of the different aggregate species formed during this process. We have investigated if different aggregates have different properties in membrane modification and how they affect cellular ROS production and calcium signalling in primary neurons and astrocytes. We have found that the effect of tau was dependent on the aggregation state of this protein and that late insoluble aggregates are able to incorporate into the membranes, activating voltage-dependent calcium channels. This in turn activates NADPH oxidase, increasing ROS production in this enzyme. Importantly, the same insoluble aggregates are able to induce cell death.

Results

In order to study the effect of the different tau aggregates on primary neuronal–astrocytic co-cultures, several batches of full length recombinant P301S tau were produced and aggregated *in vitro* in the presence of heparin as described previously [18]. The kinetics of this aggregation process are characterized by the rapid formation of thioflavin T (ThT)-active species without an apparent lag phase, with fibril formation reaching saturation after about 2 days of incubation (Fig. 1A). As expected, many filaments with a length of several micrometres could be detected in the aggregation mixtures (Fig. 1B,C). We chose different time-points (early: 30 min, 1.5, 3 and 7 h; late: 1, 3, 7, 14 and 26 days) and separated the soluble and insoluble fractions of tau to analyse the effects of the different tau species formed in the aggregation process (Fig. 1D).

Toxicity of late insoluble aggregates of tau

We first investigated if the exposure of co-cultures of primary neurons and astrocytes to the different tau aggregates had a toxic effect, and if changes in the aggregation status of tau are able to induce neuronal death. To estimate tau-induced cell death, we co-stained the cells with propidium iodide (labelling dead cells) and Hoechst (labelling the nucleus of all the cells) after 24 h of exposure to the different species: buffer (as a control), tau monomers (300 nM) and the soluble and insoluble fractions of early time-points (30 min, 1.5, 3 or 7 h) or late time-points of tau aggregation (1, 3, 7, 14, 26 days), from a corresponding monomer concentration of 300 nM (representative image in Fig. 2B). As depicted in Fig. 2A, only the

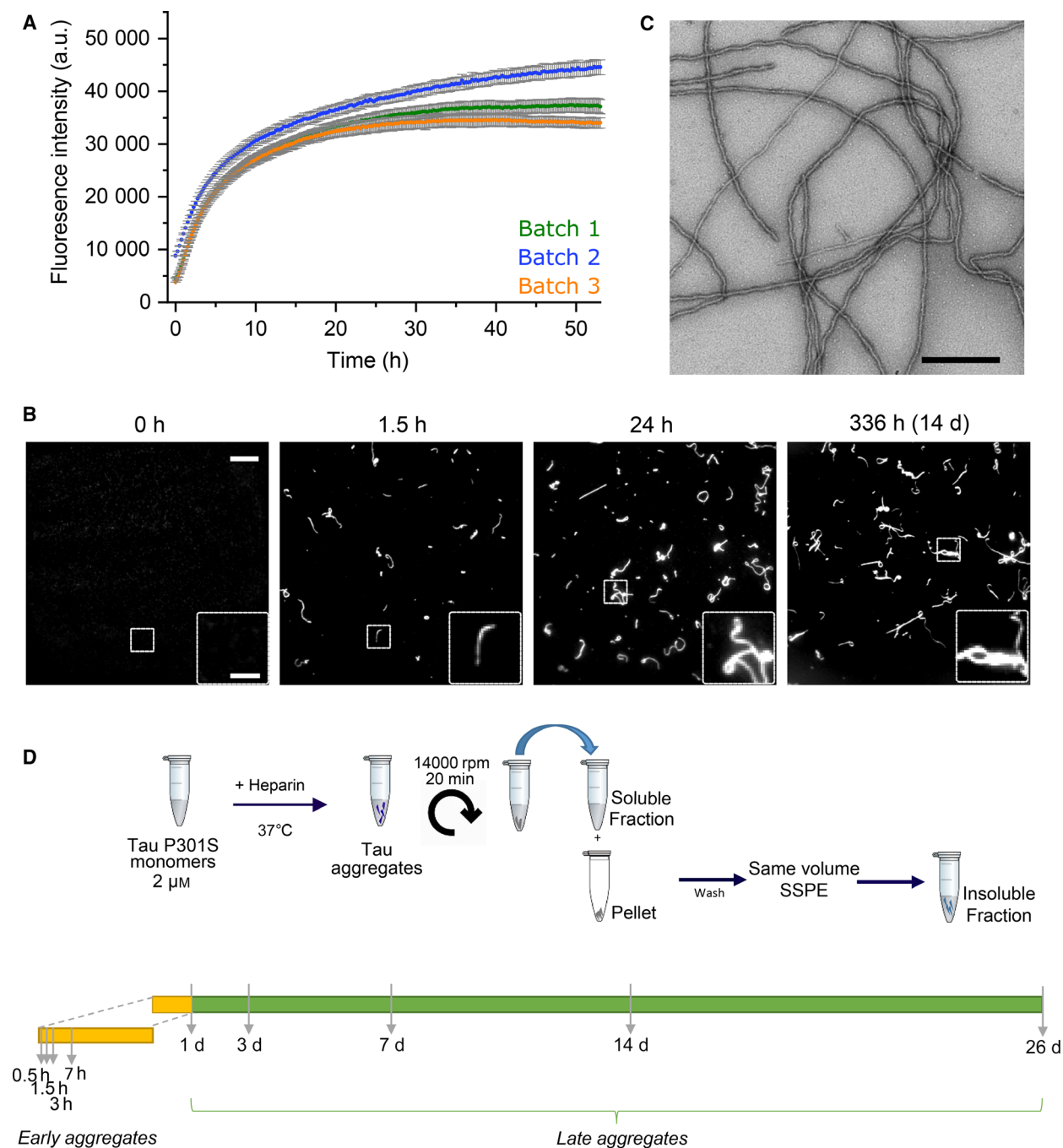


Fig. 1. Production and characterization of tau aggregates. (A) P301S tau aggregation kinetics. The extent of tau fibril formation as a function of time was monitored by measuring the fluorescence of the dye ThT over the course of the aggregation reaction. Two micromolar P301S 0N4R tau aggregation was induced by addition of $2 \mu\text{M}$ heparin. Traces for three independent experiments are shown. (B) Representative TIRFM images of fibrils (pFTAA staining) at different stages of aggregation. Scale bar $10 \mu\text{m}$, insert $2 \mu\text{m}$. (C) Representative TEM image of P301S aggregates after 7 days of aggregation. Scale bar 250 nm . (D) Schematic representation of the preparation of the different aggregates used in the study.

late insoluble aggregates were able to significantly increase cell death in the neuronal–astrocytic co-cultures, with the toxic effects increasing with aggregation

time of the protein. Compared to control ($6 \pm 2.2\%$ cell death, $n = 32$ fields analysed), the insoluble fraction of tau after 1 day of aggregation induced

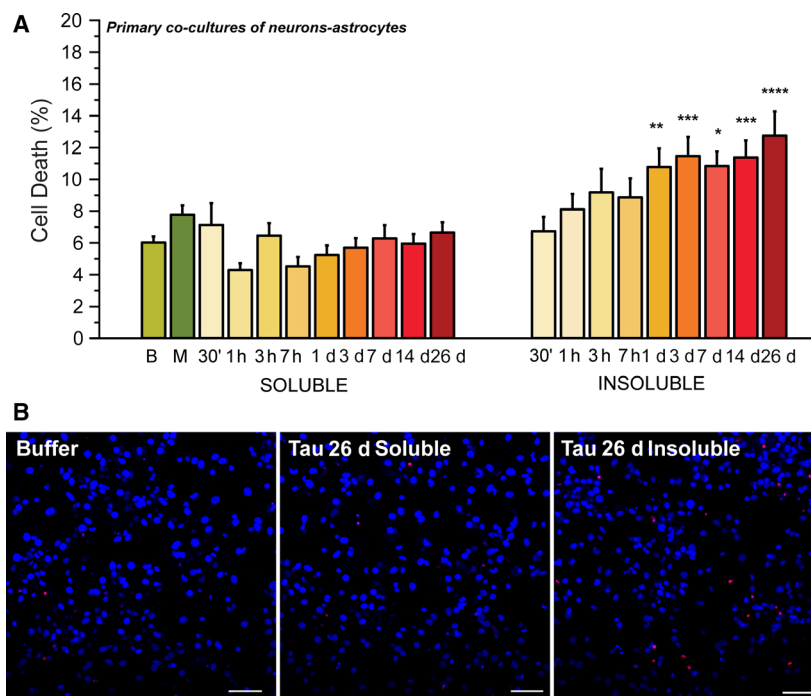


Fig. 2. Late insoluble tau aggregates induce increased rate of cell death. (A) Histograms show the quantification of tau-induced cell death in neuronal–astrocytic co-cultures after 24 h of exposure to the different tau samples (B, buffer; M, monomers). Only late insoluble aggregates (1, 3, 7, 14, 26 days) significantly induced cell death compared to control. Data are represented as mean \pm SEM. 200–400 cells were counted per field analysed (control $n = 32$, monomers $n = 11$; soluble species: tau 0.5 h $n = 11$, tau 1.5 h $n = 12$, tau 3 h $n = 13$, tau 7 h $n = 8$, tau 1D $n = 13$, tau 3D $n = 13$, tau 7D $n = 13$, tau 14D $n = 16$, tau 26D $n = 13$; insoluble species: tau 0.5 h $n = 12$, tau 1.5 h $n = 12$, tau 3 h $n = 13$, tau 7 h $n = 11$, tau 1D $n = 13$, tau 3D $n = 13$, tau 7D $n = 8$, tau 14D $n = 15$, tau 26D $n = 14$ fields). Three different sets of experiments with separate batches of protein and cell preparations were performed. One-way ANOVA with Tukey's *post hoc* comparisons ($*P < 0.05$, $**P < 0.01$, $***P < 0.0001$, $****P < 0.00001$). (B) Representative images of selected time-points of aggregation showing tau-induced cell toxicity. Cell toxicity was estimated after co-staining of the cells with propidium iodide (red fluorescence) which labels dead cells, and Hoechst (blue fluorescence) which labels all cells. Scale bar: 50 μ m.

10.7 \pm 1.2% cell death ($n = 13$, $P < 0.01$); 3-day tau induced 11.5 \pm 1.2% ($n = 13$, $P < 0.0001$); 7-day tau induced 10.9 \pm 1% ($n = 8$, $P < 0.05$); 14-day tau induced 11.4 \pm 1% ($n = 15$, $P < 0.0001$); and 26-day insoluble tau had the greatest effect with 12.8 \pm 1.5% ($n = 14$, $P < 0.00001$). Thus, only the late insoluble aggregates are able to induce an increase in the cell death in the mixed populations of cortical neurons and astrocytes, with a trend of these effects to increase as the aggregation time increases, showing the maximum effect in the latest time-point of tau aggregation.

Late insoluble aggregates elevate the rate of ROS production in primary cortical neuronal–astrocytic co-cultures

Reactive oxygen species production followed by oxidative stress is known to be one of the major triggers of neurodegeneration. We used dihydroethidium (DHE) as a ROS indicator to investigate the effects of the

different tau species in primary rat cortical co-cultures of neurons and astrocytes. Rate of increase in DHE fluorescence upon oxidation of the dye is proportional to the rate of – predominantly – superoxide generation (representative traces shown in Fig. 3B,C). After monitoring basal rate of ROS production, cells were exposed to buffer, tau monomers (300 nM), and the soluble and insoluble fractions of early time-points (30 min, 1.5, 3 or 7 h) or late time-points of tau aggregation (1, 3, 7, 14, 26 days), from a corresponding monomer concentration of 300 nM. As shown in Fig. 3A, again, only the late insoluble aggregates were able to induce a significant increase in the rate of ROS production in these cells, which is gradually increasing as tau aggregation time increases. Compared to buffer control (set as 100%, $n = 286$), the insoluble fraction of tau after 1 day of aggregation induced a rate of ROS production of 127 \pm 2.5% ($n = 182$ cells, $P < 0.0001$); insoluble tau after 3 days of aggregation 114.2 \pm 2.5% ($n = 248$ cells, $P < 0.01$); 7-day

aggregated insoluble tau induced $121 \pm 4.1\%$ ($n = 163$, $P < 0.001$); 14-day insoluble tau $125 \pm 2.9\%$ ($n = 163$, $P < 0.0001$); and 26-day insoluble tau induced the highest rate of ROS production: $131 \pm 3\%$ ($n = 289$, $P < 0.0001$). Neither the monomers, nor the soluble species nor the early insoluble aggregates induced a significant increase in the rate of ROS production in the mixed populations of cortical neurons and astrocytes compared to the control.

Aggregated tau does not induce changes in reduced glutathione level

Increased levels of ROS do not necessarily lead to pathology, as they can be quenched by effective antioxidant defences, which protect the cells from oxidative damage. One of the major markers of oxidative stress in the cells is the level of the endogenous antioxidant glutathione (GSH), so we next used the fluorescent indicator monochlorobimane to assess the levels of GSH after 24 h of incubation of the cells with early and late soluble and insoluble aggregates of tau (Fig. 3D,E). As depicted in Fig. 3D, none of the samples significantly changed the levels of GSH in the co-cultures of neurons and astrocytes. Thus, none of the tau aggregates, including late insoluble aggregates, which were able to increase the rate of ROS production, were able to induce oxidative stress. However, tau-induced ROS production can produce specific targeted oxidation of some proteins, which in combination with some other triggers (such as calcium signalling dysfunction) could lead to pathology.

Late insoluble aggregates of tau induce calcium signals in primary neurons

We next exposed the cells to the different aggregates of tau to understand if they were able to induce aberrant calcium signals in the neuronal–astrocytic co-cultures. To identify the neurons, we applied $5 \mu\text{M}$ glutamate at the end of the experiment, which induces a typical calcium response in neurons only. Application of the soluble fraction of tau (Fig. 4E) (as well as monomers, Fig. 4B) did not induce any changes in the cytosolic concentration of calcium ($[\text{Ca}^{2+}]_c$) of neurons and was comparable to the control condition (Fig. 4A), in which several neurons showed typical spontaneous oscillations. However, exposure of primary cortical co-cultures to late insoluble aggregates of tau (300 nM) induced strong characteristic peak-like calcium responses in neurons (Fig. 4C,D,F,G) but not in astrocytes (Fig. 4H–L). Importantly, the ability of tau to induce calcium signals was more pronounced as

the aggregation time of tau increased, as shown by the higher area under the curve of these responses (Fig. 5F). On the other hand, the exposition of the neurons to these tau species for ~ 20 – 30 min did not alter the amplitude of glutamate-induced calcium influx in any of the conditions (Fig. 5G).

Tau-induced calcium signals in neurons are potential-sensitive

To further characterize the calcium signal induced by the late insoluble tau aggregates, we first evaluated if the increase in $[\text{Ca}^{2+}]_c$ was dependent on extracellular calcium or calcium released from internal stores such as the endoplasmic reticulum (ER). As depicted in Fig. 5A,B, tau-induced elevation in $[\text{Ca}^{2+}]_c$ was dependent on the presence of external calcium and could be completely blocked in experiments done in Ca^{2+} -free HBSS ($+0.5 \text{ mM EGTA}$) (Fig. 5A). In addition, to exclude the effect of the intracellular stores, we used the inhibitor of SERCA thapsigargin ($0.5 \mu\text{M}$) which empties the calcium pool of the ER after 6–10 min of incubation (Fig. 5B). Subsequent addition of late insoluble aggregated tau (300 nM) to these cells induced calcium signals in neurons similar to the obtained in the absence of thapsigargin (Fig. 4G) which confirms that tau-induced $[\text{Ca}^{2+}]_c$ rise in neurons is independent of intracellular Ca^{2+} stores.

Extracellular Ca^{2+} could enter the cytosol through plasmalemmal calcium channels, either native or formed by tau. Voltage-gated calcium channels (VGCC) are one of the major sources of extracellular Ca^{2+} influx in neurons. These ionic channels are potential sensitive, as are normally closed at resting membrane potential and activated on plasma membrane depolarization. To test their contribution to the tau-induced calcium signals in our neurons, we used two different antagonists of these channels. We first applied nifedipine $5 \mu\text{M}$ to the cells during the measurement, once the tau-induced calcium signals had already begun. This greatly diminished the $[\text{Ca}^{2+}]_c$ increases induced by the late insoluble aggregates of tau (Fig. 5C). A similar reduction was observed when preincubating the cells with this VGCC inhibitor before the addition of the late insoluble tau aggregates (Fig. 5D – as compared with the tau response showed in Fig. 4F – and 5F). Likewise, preincubation of the primary co-culture of neurons and astrocytes with the VGCC antagonist verapamil ($20 \mu\text{M}$) completely blocked the $[\text{Ca}^{2+}]_c$ elevation induced by insoluble aggregates (Fig. 5E,F). Thus, insoluble aggregates of tau activate potential sensitive calcium channels and induce calcium signals specifically in neurons.

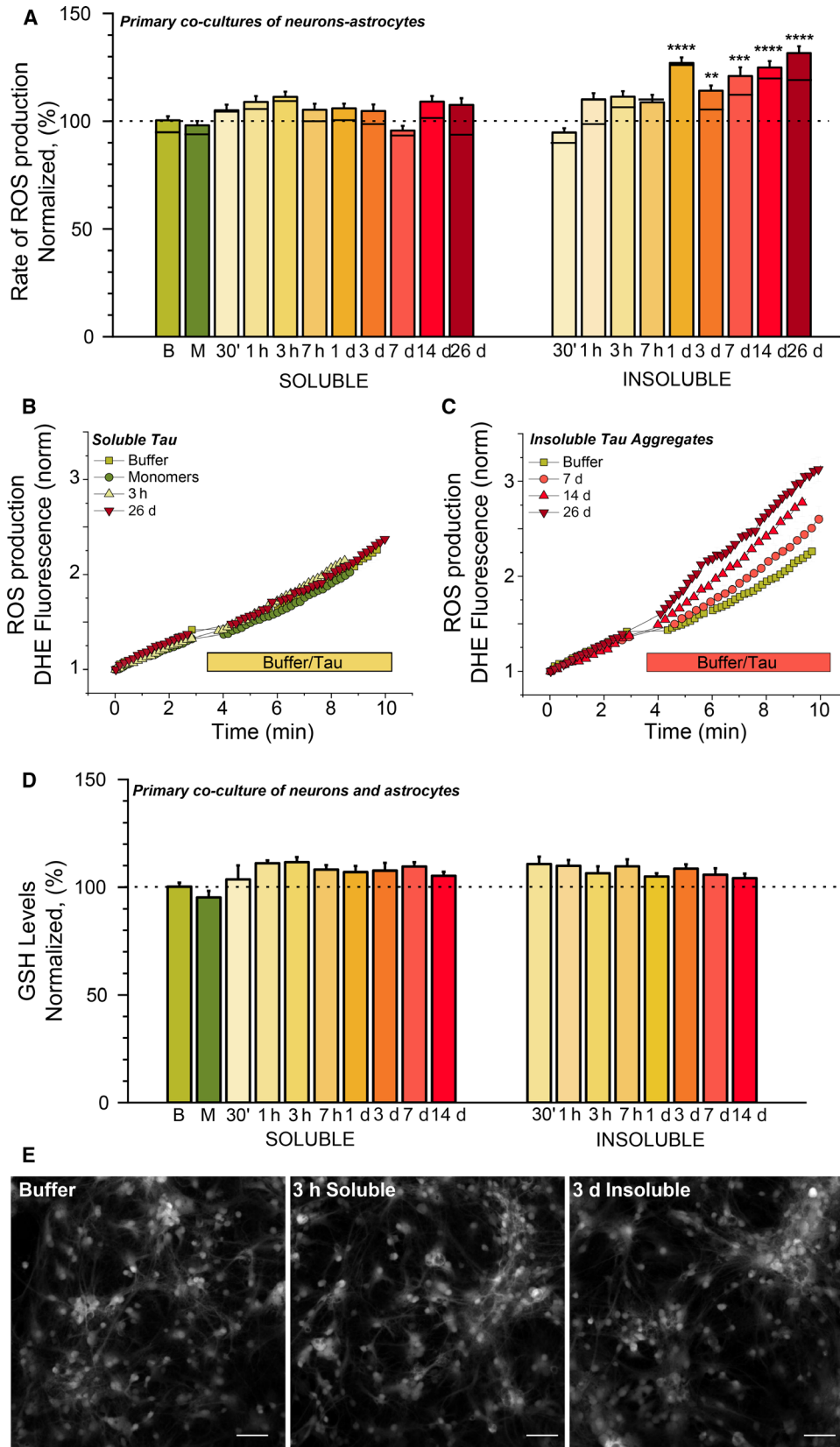


Fig. 3. Late insoluble aggregates induce increased rate of ROS production. (A) Histograms represent the increase in the rate of ROS production after extracellular application of tau to cortical primary cultures (B, buffer; M, monomers). Rate of ROS production is reflected by the rate of DHE fluorescence as explained in [Materials and methods](#). Data are represented as mean \pm SEM, and black line represents median. $n = \sim 150$ –300 neurons + astrocytes were analysed in three different set of experiments with separate batches of protein and cell preparations: (control $n = 286$, monomers $n = 191$; soluble species: tau 0.5 h $n = 184$, tau 1.5 h $n = 191$, tau 3 h $n = 177$, tau 7 h $n = 163$, tau 1D $n = 233$, tau 3D $n = 189$, tau 7D $n = 188$, tau 14D $n = 169$, tau 26D, $n = 249$; insoluble species: tau 0.5 h $n = 154$, tau 1.5 h $n = 197$, tau 3 h $n = 184$, tau 7 h $n = 164$, tau 1D $n = 182$, tau 3D $n = 248$, tau 7D $n = 163$, tau 14D $n = 163$, tau 26D $n = 289$). Nonparametric Kruskal–Wallis H test was used to determine statistical significances, $**P < 0.01$, $***P < 0.001$, $****P < 0.0001$. (B, C) Representative traces showing DHE fluorescence increase, which is proportional to the rate of ROS production. Only application of late insoluble aggregates (C) induces an increase in the rate of ROS production. (D) Histograms show the quantification of GSH levels (MCB fluorescence) in neuronal–astrocytic co-cultures after 24 h of exposure to the different tau samples (B, buffer; M, monomers). None of them induced significant changes in GSH levels. Three different sets of experiments with separate batches of protein and cell preparations were performed. Data represented as mean \pm SEM of $n = \sim 10$ –20 fields analysed: (control $n = 20$, monomers $n = 15$; soluble species: tau 0.5 h $n = 11$, tau 1.5 h $n = 11$, tau 3 h $n = 10$, tau 7 h $n = 11$, tau 1D $n = 15$, tau 3D $n = 14$, tau 7D $n = 16$, tau 14D $n = 16$; insoluble species: tau 0.5 h $n = 12$, tau 1.5 h $n = 11$, tau 3 h $n = 12$, tau 7 h $n = 15$, tau 1D $n = 15$, tau 3D $n = 9$, tau 7D $n = 16$, tau 14D $n = 19$). (E) Representative images showing a field of cells depicting MCB fluorescence (z-projection from corresponding z-stacks). Scale bar: 50 μm .

Increase in $[\text{Ca}^{2+}]_c$ can lead to the activation of different cellular pathways, such as PKC, which in turn may lead to the activation of different enzymes such as NADPH oxidase (NOX). In neurons and astrocytes, NOX, together with mitochondria, is one of the major sources of ROS [3,19]. To understand if this was the case in our study, we selected the late insoluble aggregate tau 14D (14 days aggregation), which was able to induce a strong increase in ROS production (Fig. 2A) and calcium signals (Fig. 4G). Preincubation of the primary co-culture of neurons and astrocytes with the inhibitor of NADPH oxidase 20 μM AEBSF for 20 min completely blocked the increase in the rate of ROS production induced by the 14D insoluble fraction of tau (Fig. 5H,I, Control $100 \pm 6\%$, $n = 89$; Tau $154 \pm 5\%$, $n = 112$; AEBSF $105 \pm 3\%$ $n = 122$, $P < 0.00001$), confirming that insoluble aggregates of tau produce ROS in neurons and astrocytes through the activation of NADPH oxidase. In addition, nifedipine (5 μM), which inhibited the calcium signals induced by late insoluble tau aggregates (Fig. 5C,D), was also able to block the ROS production induced by the same tau species (Fig. 5F, G, 85 ± 11 , $n = 98$, $P < 0.00001$), thus providing a link between the late insoluble tau-induced calcium signals and the increased rate of ROS production.

Late insoluble tau aggregates induce electrophysiological activity in artificial membranes

One of the possible mechanisms of tau action on the cells might be through its ability to directly induce an increase in cell membrane permeability. To test this possibility, we studied the effects of tau aggregates on

the ion conductance of planar bilayer lipid membranes. Electrophysiological activity was recorded for monomers, 3 h soluble aggregates, and late soluble and insoluble aggregates (3D, 5D, 7D, 12D). Introduction of the insoluble aggregates into the lipid bilayer caused a gradual increase in the membrane conductance (Fig. 6A). Such an insertion suggests that, unlike traditional channels exerting a stepwise insertion, the interaction of tau aggregates with the lipid bilayer may be of a type which more closely resembles ionophore activity with gradual increase in the membrane conductance. In control experiments, we tested channel membrane conductance in the presence of the soluble fractions which did not exhibit any effects on the membrane conductance (Fig. 6B) confirming that insoluble aggregates are responsible for the interaction with the membranes.

While all aggregated fractions demonstrated increased conductance, its value and properties were distinct depending on the time-point of aggregation. As it can be seen from Fig. 6C,D both detection frequency and conductance values increased with the increase in aggregation times. Importantly in the samples that were aggregated for longer periods of time, we detected two models of voltage-dependent behaviour. Some channels were not voltage dependent (Fig. 6E) while others demonstrated strong rectification at the negative voltages (Fig. 6F). The higher the aggregation time the wider was the conductance distribution and higher the occurrence of nonlinear trends in the I/V curves. Both behaviours can potentially be related to the variable size of the aggregates. Voltage-dependent channel rectification indicates that tau species linked to such behaviour most likely can interact and insert into the lipid bilayers in a voltage-

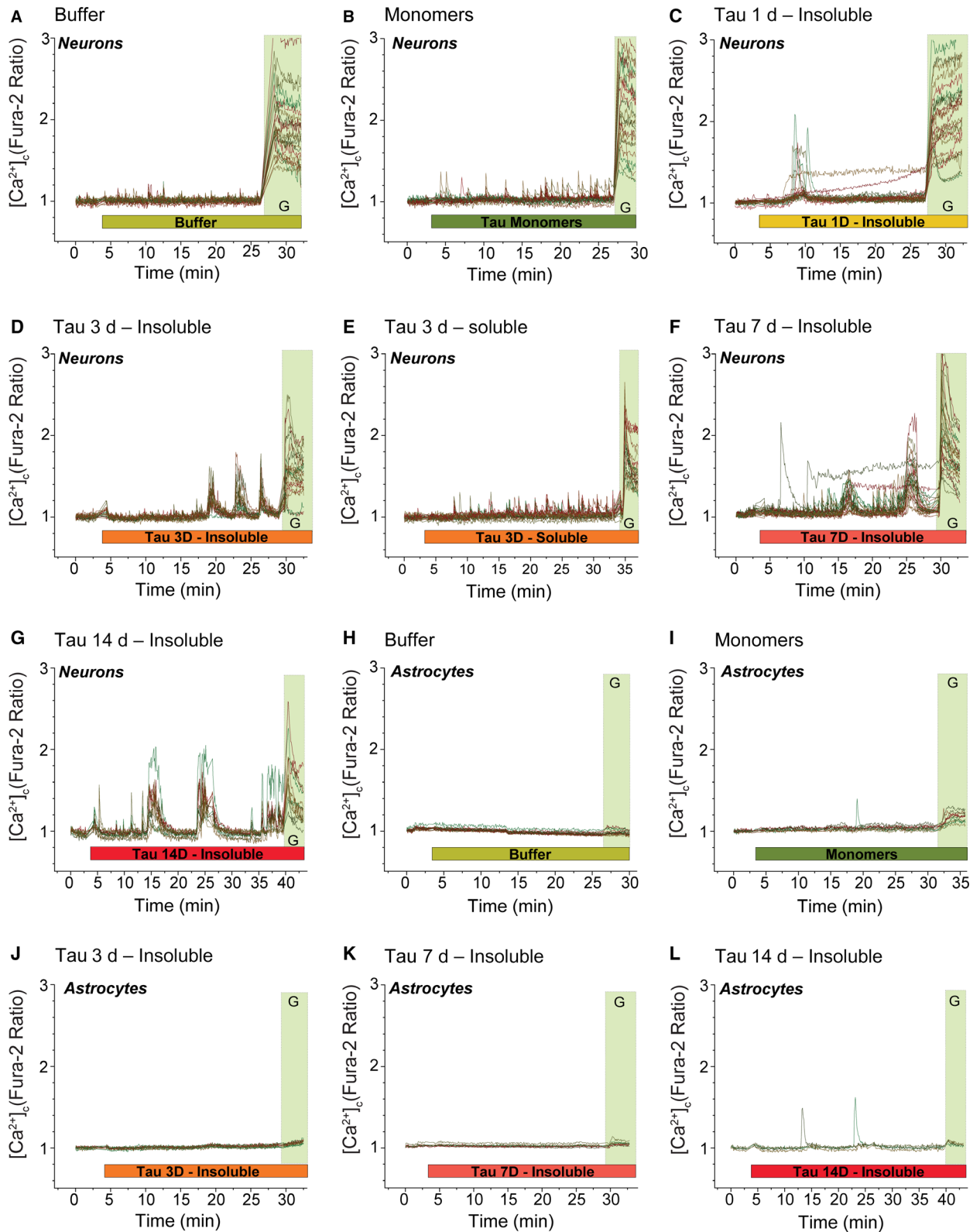


Fig. 4. Late insoluble tau aggregates induce calcium signals in neurons. Representative traces showing the cytosolic calcium levels measured by Fura-2 ratio in individual neurons (A–G) and astrocytes (H–L) in response to the different tau samples. Typically, representative traces for 20–30 cells are shown per condition. Glutamate 5 μ M (G) was added at the end to identify neurons.

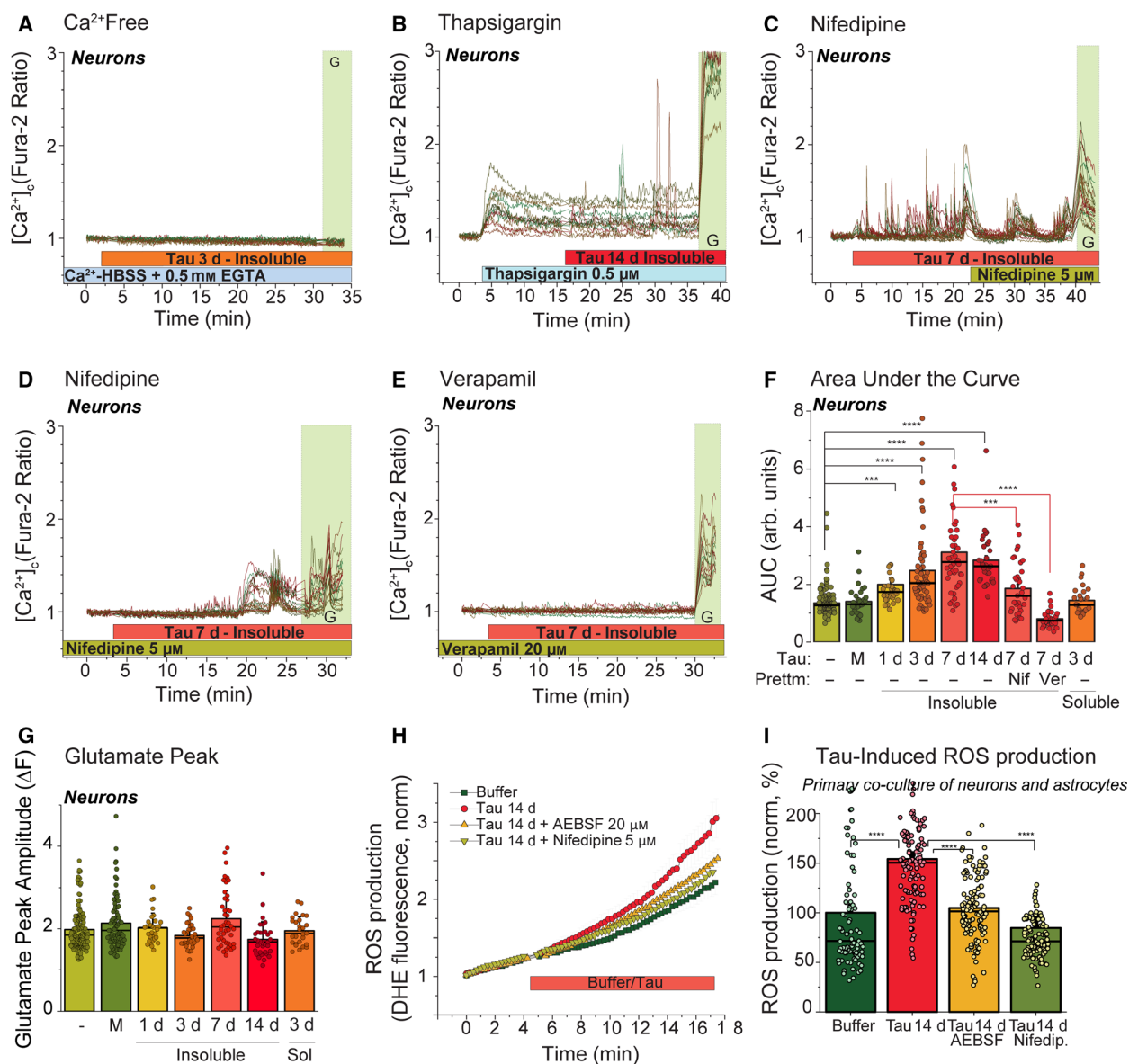


Fig. 5. Tau-induced calcium signals in neurons are potential-dependent. (A–E) Representative traces showing the cytosolic calcium levels measured by Fura-2 in individual neurons (20–30 cells) in different conditions. (A) Cells were preincubated in calcium-free HBSS supplemented with 0.5 mM EGTA to study if the tau-induced signals depended on extracellular calcium. (B) Cells were treated with thapsigargin 0.5 μM for 10 min before the application of tau to inhibit SERCA pump and study the contribution of the ER to the calcium signals. (C) Cells were treated with 5 μM nifedipine to inhibit the VGCC after tau-induced calcium signals started. (D, E) Cells were pretreated with 5 μM nifedipine or 20 μM verapamil to inhibit the VGCC before the application of tau. (F) Histograms represent the quantification of the area under the curve of the different calcium signals, $n = 18$ –140 cells analysed, each shown as a dot (control $n = 146$, monomers $n = 32$, insoluble tau 1D $n = 31$, tau 3D $n = 62$, tau 7D $n = 45$, tau 14D $n = 34$, tau 7D + nifedipine $n = 35$, tau 7D + verapamil $n = 34$, soluble tau 3D $n = 27$). Data are represented as mean \pm SEM, and black lines represent median. Nonparametric Kruskal–Wallis H test was used to determine statistical significances, $***P < 0.001$, $****P < 0.0001$. (G) Amplitude of the calcium increase induced by glutamate, $n = 27$ –146 cells analysed, each shown as a dot (control $n = 146$, monomers $n = 83$, tau 1D $n = 31$, tau 3D $n = 33$, tau 7D $n = 45$, tau 14D $n = 34$, tau 3D soluble $n = 27$). Data are represented as mean \pm SEM, and black lines represent median. Nonparametric Kruskal–Wallis H test was used to determine statistical significances (nonsignificant differences found). (H) Representative traces showing DHE fluorescence increase as a marker of ROS production in primary co-cultures of neurons and astrocytes after application of buffer or insoluble Tau 14D with or without preincubation with the NOX inhibitor AEBFSF 20 μM or the voltage-dependent calcium channel inhibitor nifedipine 5 μM. (I) Histograms represent the increase in the rate of ROS production after extracellular application of buffer/tau to cortical primary cultures in the conditions explained in H. Data are presented as mean \pm SEM, and black lines represent median. $n = 89$ –122 cells analysed, each represented as a dot (control $n = 89$, tau 14D $n = 112$, tau 14D + AEBFSF $n = 122$, tau 14D + nifedipine $n = 98$). Nonparametric Kruskal–Wallis H test was used to determine statistical significances, $****P < 0.0001$.

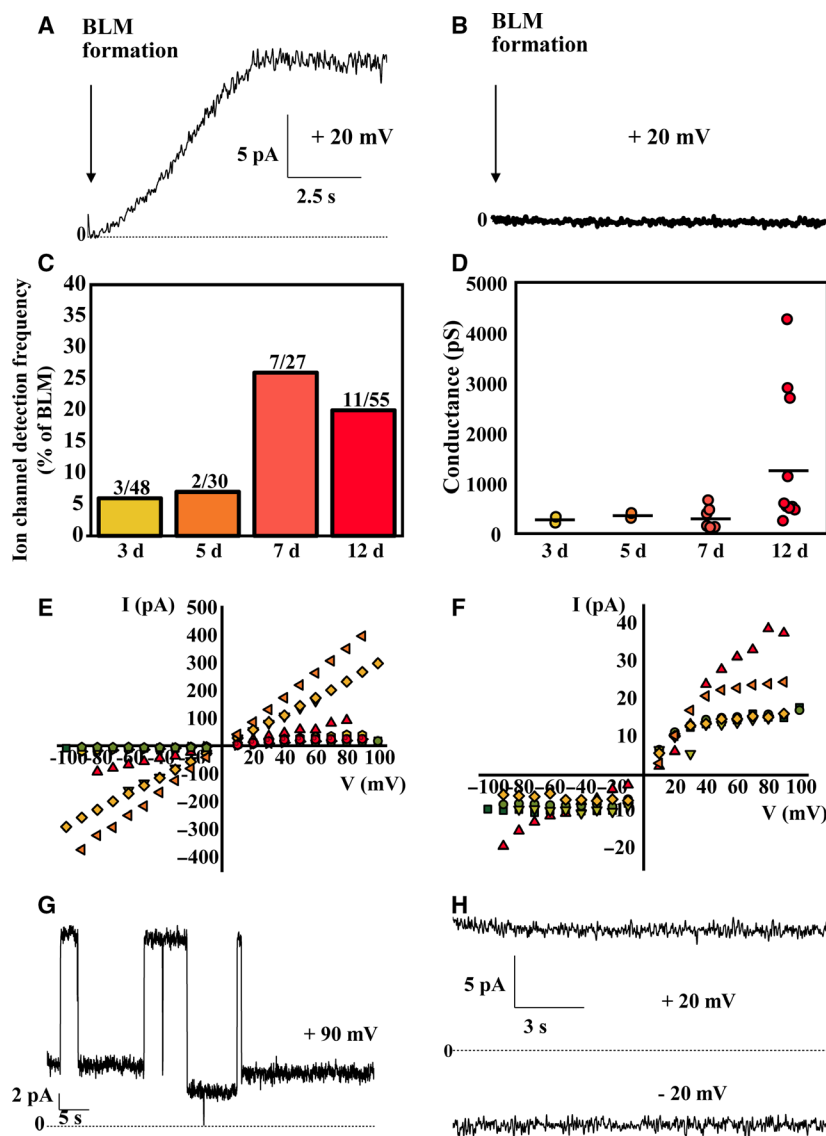


Fig. 6. Late insoluble tau aggregates induce electrophysiological activity in artificial membranes. (A) Representative trace showing increase in ion conductance due to the insertion of insoluble tau aggregates as compared to (B), a control trace of the bilayer with no protein present. (C) Histogram showing the ion channel detection frequency of tau aggregates related to their incubation period ($n = 48$ independent recordings for tau 3D, $n = 30$ for tau 5D, $n = 27$ for tau 7D, $n = 55$ for tau 12D). (D) Open channel conductance point distributions of tau aggregates at different incubation stages (tau 3D $n = 3$, tau 5D $n = 2$, tau 7D $n = 7$, tau 12D $n = 11$). (E) IV curve of the 12D aggregates showing a linear behaviour as compared to (F), 12D aggregates with nonlinear behaviour. (G) Representative trace of 3D tau aggregates channel responding to high voltage by switching to lower conductance states. (H) Representative trace of a 12D aggregate showing a nonlinear behaviour. Four different batches of aggregated tau were used.

dependent manner. Interestingly, the 3D aggregate, despite its low-frequency detection (Fig. 6C), was able to form a typical channel with an increased spontaneous openings and closures at higher voltages (Fig. 6G) while longer aggregated proteins did not demonstrate channel activity (Fig. 6H).

Discussion

The role of extracellular tau in pathology has recently gained increasing interest, especially in the context of the prion-like spreading of tau pathology through the brain. Here, we show that in addition, extracellular tau aggregates also exert a direct pathogenic effect in neuronal-astrocytic cultures, and, more importantly, these effects directly depend on the stage of tau

aggregation. One of the most important findings in our study is that despite sharing a β -sheet structure, the various tau aggregates formed during the aggregation process have different biological and pathological activities. This can partially explain the diversity of results obtained in different laboratories regarding the toxicity/pathogenesis of tau.

Our results show that only late insoluble aggregates (formed after 24 h of *in vitro* aggregation) have toxic effects in the cultures and induce ROS production through NOX, calcium signals in the neurons, and alter the permeability of lipid bilayer membranes. ThT staining shows that around this time-point the fibrils' formation reaches the saturation point. Interestingly, the tau-induced effects tended to increase as the time of aggregation increased. We showed recently the

kinetics and characterization of the aggregation reaction and found that mutant P301S tau, the one used for this study, elongates fast (around 24 h) into long fibrils and then enters a stage of spontaneous slow fibril fragmentation in which fibrils decrease in length over time [18]. This suggests that not only the structure, but also the length of the fibrils might influence its activity, with shorter fibrils being more effective at inducing the pathogenic effects shown than longer fibrils.

Previous work from other groups has shown that the species formed by *in vitro* heparin-induced aggregation of tau share many similarities but might also differ in some aspects with the fibrils found in the brains from patients or transgenic animal models. At a specific time-point, heparin-aggregated tau has been shown to have a different conformation and seeding capacity [20] or a different cryo-EM structure [21] than native fibrils. Additionally, tau samples used in our study are not phosphorylated. These studies and the present manuscript highlight how critical the stage of *in vitro* tau aggregation might be for the effects studied; the link between tau mutations, filament structure and disease-specificity; and the complexity and variability of conformations in which tau can be present.

In our study, insoluble aggregates of tau induced a significant increase in the percentage of dead neurons and astrocytes. However, the effect of tau is much smaller compared to oligomeric β -amyloid or α -synuclein [14,22]. The importance of tau aggregation in the induction of cell death was also shown previously in a cell model of tauopathy, where inhibitors of tau aggregation prevented cell death [23].

The ability of endogenous tau to induce ROS in mitochondria has been shown for several tauopathies [1,2,24], and we cannot exclude the effect of tau on mitochondria in our experiments. However, most of the ROS production induced by tau in our cells was dependent on NADPH oxidase, as shown by the dramatic reduction in the rate of ROS production in the presence of the NADPH oxidase inhibitor AEBSEF. Although activation of NADPH oxidase was shown for transgenic models of AD, the direct effect of tau on ROS production in NOX enzymes was not shown before. However, here we demonstrated that tau-induced ROS production can be blocked by the VGCC inhibitor nifedipine suggesting that NADPH oxidase is activated by the calcium influx through potential sensitive calcium channels. As shown before, in neurons and astrocytes, NADPH oxidase can be activated by Ca^{2+} [19]

The effect of tau on $[\text{Ca}^{2+}]_c$ is dependent on the membrane activity in our experiments. Nonlinear

trends in I/V curves suggest that tau aggregates incorporate into the membrane depending on charge. Incorporation of aggregated tau into the membrane induced integral conductance which in some form can be described as a channel (Fig. 6A). It is more likely to be selective for K^+ (what we show) or to other monovalent cations and less likely to be selective to Ca^{2+} because it would stimulate calcium signal independently of the activation of the potential sensitive calcium channels.

Acute extracellular application of P301S tau monomers did not induce any immediate calcium signals in the neurons, in agreement with recent results from our group using monomers from the K18 tau fragment, corresponding to the 4R region of the protein [25]. We previously showed however that a longer exposure (24 h) of the cells to the K18 monomers induced calcium oscillations and impaired the glutamate-induced calcium signalling in the neurons [25]. None of the tau species tested in the present manuscript affected the amplitude of the glutamate-induced calcium signals in the neurons after a short exposition (20–30 min). Further characterization will be necessary to study the effects of the different tau species in the impairment of the glutamate-induced calcium signalling, the possible tau isoform specificity, and/or the requirement of a longer incubation time and probably the internalization of the protein.

Tau monomers and fibrils are indeed efficiently uptaken by cells [20]. However, in the present scenario, the cellular effects induced by tau fibrils are more likely to occur from the extracellular site where they were applied given the immediacy of the responses. Nevertheless, the ability of tau fibrils to interact with the plasma membrane and modify its permeability might also occur from the intracellular side and be induced either by endogenous or uptaken tau.

In summary, our results show a mechanism summarized in Fig. 7 by which specific extracellular tau aggregates can lead to neurodegeneration and contribute to the pathogenesis of tauopathies.

Materials and methods

Cell culture

Co-cultures of cortical neurons and astrocytes were prepared as described previously [26] from Sprague-Dawley rat pups (P3–P4) from the UCL breeding colony. Experimental procedures were performed in full compliance with the United Kingdom Animal (Scientific Procedures) Act of 1986 and with the European directive 2010/63/EU, approved by the UCL Animal Welfare and Ethical Review Body and

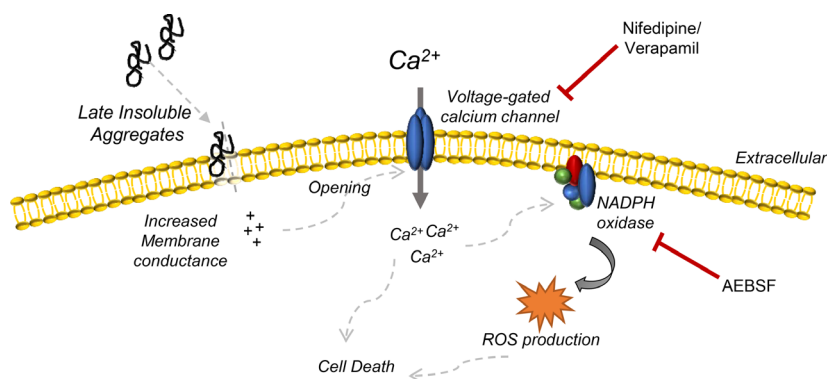


Fig. 7. Extracellular late insoluble tau aggregates effects in cells. Schematic diagram of extracellular late insoluble tau aggregates effects in cells. Our results suggest that specific aggregates of tau (insoluble species formed after at least 24 h of *in vitro* aggregation) are able to interact with lipid membranes and alter their membrane conductance. This induces the opening of VGCC allowing Ca^{2+} influx in the neurons, which in turn activates NADPH oxidase (NOX), increasing ROS production through this enzyme. Nifedipine, a VGCC blocker, is able to prevent both the calcium signals and the ROS production induced by tau, while AEBSF, a NOX inhibitor, greatly diminishes ROS production. The combination of all these effects is likely leading to cell death, as only the same insoluble aggregates were shown to be toxic to the primary neuronal–astrocytic co-cultures.

granted by the corresponding personal, project and establishment licenses. Cortex was dissected and placed in ice-cold PBS. Tissue was then trypsinized for 15 min at 37 °C, triturated and plated in coverslips that were previously coated with Poly-D-Lysine. Cultures were maintained in Neurobasal A medium, supplemented with B-27, Gluta-MAX and in the presence of penicillin/streptomycin (all of them from Thermo Fisher Scientific, Paisley, UK). Media were replaced after 1 week, and cells were used at 12–16 DIV in all the experiments.

Tau samples preparation and characterization

Recombinant P301S Tau was purified and aggregated as previously described [18]. In brief, the aggregation of 2 μM P301S tau in 1 \times SSPE buffer (20 mM phosphate, 298 mM NaCl and 2 mM EDTA, pH 8) was induced by addition of 2 μM low molecular weight (~ 5000 Da) heparin (Thermo Fisher). The mixture was then incubated under quiescent conditions at 37 °C for the indicated periods of time.

To separate insoluble and soluble fractions, aliquots were taken from the aggregation mixture and centrifuged at 21 000 *g* for 20 min prior to the experiment. The insoluble fraction was further washed once with SSPE buffer, before resuspending it in the original volume of SSPE. Several independent batches of protein were used for these experiments.

Aggregate characterization by SAVE imaging

SAVE images were acquired as described previously [18]. Briefly, samples were diluted into 30 nM pFTAA to a final protein concentration of 50 nM. Then, 10 μL of each

sample was adsorbed to borosilicate cover slides no. 1.5 for 15 min and imaged on a TIRF setup using 488 nm excitation.

Aggregate characterization by transmission electron microscopy

Samples were placed on glow-discharged 400 meshed Formvar/carbon film-coated copper grids (Sigma-Aldrich, Gillingham, UK) for 3 min and stained with uranyl acetate. Images were taken on a Philips Spirit transmission electron microscope at a magnification of 9600 \times .

Monitoring fibril formation by ThT assay

To monitor the fibril formation of tau, 10 μM ThT was added to the aggregation mixtures prior to each measurement. Samples were thoroughly mixed by inverting the tubes and placed into a COSTAR half-area 96-well plate in triplicates. The plate was incubated at 37 °C without shaking for the indicated duration. The samples were excited at 440 nm, and fluorescence was monitored at 480 nm using aFLUOstar OPTIMA plate reader (BMG LabTech, Ortenberg, Germany).

Live cell imaging

Experiments were performed in HBSS buffer (with Ca^{2+} and Mg^{2+}) supplemented with 10 mM HEPES and adjusted to pH 7.4. In specific experiments indicated in the text, calcium-free HBSS was used, consisting on commercial Ca^{2+} and Mg^{2+} -free HBSS supplemented with 2 mM MgCl_2 and 0.5 mM EGTA.

Cell death

Three hundred nanomolar of the different tau time-points samples or the same volume of SSPE buffer as a control was applied to the extracellular medium of the primary neuronal–astrocytic cultures and incubated for 24 h. Cells were then loaded for 15 min with 20 μM propidium iodide and 10 μM Hoechst 33342. While Hoechst is a blue fluorescent dye that stains chromatin DNA, propidium iodide is only permeable to dead cells and shows red fluorescence, so it is possible to calculate the percentage of dead cells (showing red fluorescence) versus total number of cells (showing blue fluorescence). Images were acquired in a Zeiss 710 LSM confocal microscope (Carl Zeiss, Oberkochen, Germany) with an integrated META detection system using a 20 \times objective. Samples were excited at 405 and 561 nm, and emission light was collected at 430–460 nm and above 590, respectively. Images were analysed using IMAGEJ (NIH, Bethesda, MD, USA). A total number of 800–1000 cells were counted in 4–5 different fields per coverslip. Experiments were repeated three times with different batches of protein and separate independent cultures.

ROS production

Reactive oxygen species production was monitored in single cells using the superoxide indicator DHE (2 μM ; Molecular Probes, Thermo Fisher Scientific, Waltham, MA, USA), which shows blue fluorescence in the cytosol until oxidized, when it intercalates within the DNA, staining the nucleus fluorescent red. Fluorescence measurements were made on an Nikon Eclipse Ti-S (Nikon Imaging, Tokyo, Japan) epifluorescence inverted microscope equipped with a 20 \times fluorite objective. Excitation light was provided by a xenon arc lamp, the beam passing a monochromator to provide excitation light at 530 nm (Cairn Research, Kent, UK). Emitted fluorescence light was reflected through an ET605/52m filter to an Andor Zyla sCMOS camera (Cairn Research) and digitized to a 16-bit resolution. All imaging data were collected and analysed using ANDOR IQ2 (Andor, Belfast, UK) and ORIGIN PRO 2018 (Origin Lab, Northampton, MA, USA) software. Basal rate of ROS production, measured as the rate of increase in red DHE fluorescence, was immediately recorded after dye-loading for 3 min. Three hundred nanomolar of the different tau samples or the same volume of SSPE buffer as a control was then applied to the extracellular medium of the primary neuronal–astrocytic culture, and rate of ROS production was recorded for several minutes more. Ratio of the rate of ROS production after stimulation with tau or buffer *vs* basal rate of ROS was calculated for each time-point of tau aggregation and normalized to control. Around 150–300 cells (neurons + astrocytes) were analysed in each condition. Experiments were repeated three times with different batches of protein and separate cultures.

Glutathione

Three hundred nanomolar of the different tau samples or the same volume of SSPE buffer as a control was applied to the extracellular medium of the primary neuronal–astrocytic culture and incubated for 24 h prior the experiments. To analyse glutathione (GSH) levels, cells were incubated with 50 μM monochlorobimane (MCB) in HBSS at room temperature for 30 min. Cells were then washed with HBSS, and live-cell images were acquired in a Zeiss 710 LSM confocal microscope equipped with a META detection system, using an EC Plan-Neofluar 40 \times objective. MCB was excited at 405 nm, and emission light was detected between 430 and 525 nm. Z-stacks were acquired, and fluorescence intensity was analysed using VOLOCITY 3D Image Analysis Software (PerkinElmer, Waltham, MA, USA). Experiments were repeated three times with different batches of protein and separate independent cultures.

[Ca²⁺]_c imaging

[Ca²⁺]_c was monitored in single cells using Fura-2 AM, a high-affinity intracellular calcium indicator which is ratiometric and allows an accurate measurement of the cytosolic Ca²⁺ as the ratio of the emissions of the dye in response to 340/380 excitation, independently of loading variations. Cells were loaded for 30 min at room temperature with 5 μM fura-2 AM in the presence of 0.0005% pluronic in HBSS buffer. Fluorescence measurements were made on an epifluorescence inverted microscope equipped with a 20 \times fluorite objective (Nikon Eclipse Ti-S). Excitation light was provided by a xenon arc lamp, the beam passing a monochromator at 340 and 380 nm (Cairn Research). Emitted fluorescence light was reflected through an ET510/80m filter to an Andor Zyla sCMOS camera (Cairn Research) and digitized to a 16-bit resolution. All imaging data were collected and analysed using ANDOR IQ2 (Andor) and ORIGIN PRO 2018 (Origin Lab) software. Area under the curve (mathematical area) was calculated with the integration function in ORIGIN PRO 2018, using a constant number of frames and after baseline subtraction.

BLM recordings

Tau aggregates were resuspended into 20 mM Tris and 0.05% Genapol at a final concentration of 300 nM. The painting method was used to form phospholipid bilayer using 1,2-diphytanoyl-*sn*-glycero-3-phosphocholine (DiPhPC; Avanti Polar Lipids, Alabaster, AL, USA). A Delrin cuvette with an aperture of 50 μm diameters was placed between the two chambers of the Teflon cuvette. The aperture was pre-painted with 25 mg·mL⁻¹ of DiPhPC in decane. 150 mM KCl and 20 mM HEPES, pH 5, was used as the recording solution and added to both sides of the chamber. Ion currents were detected using standard

Ag-AgCl electrodes (World Precision Instruments, Sarasota, FL, USA) that were placed in each side of the cuvette. Measurements of the conductance of single channels were performed by painting the protein to the *cis* side of the chamber (side connected to the ground electrode). Conductance measurements were performed using an eONE amplifier (Elements, Cesena, Italy) with a sampling rate of 1.22 kHz (819.20 μ s interval). Signals were filtered by low-pass Bessel filter at 20 Hz for analyses performed with ORIGINPRO 2019 (Origin Lab) and CLAMPFIT software (Molecular Devices, San Jose, CA, USA).

Statistics

Statistical analysis was performed with ORIGINPRO 2018 and IBM STATISTICS SPSS 24 (IBM, Armonk, NY, USA). Data sets were first probed for normality with the Shapiro–Wilk test, and homogeneity of variances was analysed with Levene's test. When the data sets did not follow a normal distribution, nonparametric tests were performed (Kruskal–Wallis *H* test). When appropriate, one-way ANOVA followed by *post hoc* Tukey test was used. Differences were considered to be significantly different if $P < 0.05$.

Acknowledgements

NE: Postdoctoral Fellowship Fundacion Alfonso Martin-Escudero (Spain). The work was supported by EPSRC grant EP/R024898/1.

Conflict of interest

The authors declare no conflict of interest.

Author contributions

AYA, NE, FK and DK conceptualized the study. NE, FK and GFA performed and analyzed the experiments and prepared the figures. EVP, DK and AYA provided the resources and the funding. AYA and NE wrote the original draft. NE, FK, GFA, EVP, DK and AYA wrote, reviewed and edited the manuscript.

References

- Angelova PR, Barilani M, Lovejoy C, Dossena M, Vigano M, Seresini A, Piga D, Gandhi S, Pezzoli G, Abramov AY *et al.* (2018) Mitochondrial dysfunction in Parkinsonian mesenchymal stem cells impairs differentiation. *Redox Biol* **14**, 474–484.
- Esteras N, Rohrer JD, Hardy J, Wray S & Abramov AY (2017) Mitochondrial hyperpolarization in iPSC-derived neurons from patients of FTDP-17 with 10+16 MAPT mutation leads to oxidative stress and neurodegeneration. *Redox Biol* **12**, 410–422.
- Gandhi S & Abramov AY (2012) Mechanism of oxidative stress in neurodegeneration. *Oxid Med Cell Longev* **2012**, 428010.
- Esteras N, Dinkova-Kostova AT & Abramov AY (2016) Nrf2 activation in the treatment of neurodegenerative diseases: a focus on its role in mitochondrial bioenergetics and function. *Biol Chem* **397**, 383–400.
- Abramov AY, Canevari L & Duchen MR (2004) Beta-amyloid peptides induce mitochondrial dysfunction and oxidative stress in astrocytes and death of neurons through activation of NADPH oxidase. *J Neurosci* **24**, 565–575.
- Abramov AY & Duchen MR (2005) The role of an astrocytic NADPH oxidase in the neurotoxicity of amyloid beta peptides. *Philos Trans R Soc Lond B Biol Sci* **360**, 2309–2314.
- Deas E, Cremades N, Angelova PR, Ludtmann MH, Yao Z, Chen S, Horrocks MH, Banushi B, Little D, Devine MJ *et al.* (2016) Alpha-synuclein oligomers interact with metal ions to induce oxidative stress and neuronal death in Parkinson's disease. *Antioxid Redox Signal* **24**, 376–391.
- Ludtmann MHR, Angelova PR, Horrocks MH, Choi ML, Rodrigues M, Baev AY, Berezhnov AV, Yao Z, Little D, Banushi B *et al.* (2018) alpha-synuclein oligomers interact with ATP synthase and open the permeability transition pore in Parkinson's disease. *Nat Commun* **9**, 2293.
- Angelova PR & Abramov AY (2017) Alpha-synuclein and beta-amyloid – different targets, same players: calcium, free radicals and mitochondria in the mechanism of neurodegeneration. *Biochem Biophys Res Comm* **483**, 1110–1115.
- Arispe N, Rojas E & Pollard HB (1993) Alzheimer disease amyloid beta protein forms calcium channels in bilayer membranes: blockade by tromethamine and aluminum. *Proc Natl Acad Sci USA* **90**, 567–571.
- Abramov AY, Canevari L & Duchen MR (2003) Changes in intracellular calcium and glutathione in astrocytes as the primary mechanism of amyloid neurotoxicity. *J Neurosci* **23**, 5088–5095.
- Abramov AY, Ionov M, Pavlov E & Duchen MR (2011) Membrane cholesterol content plays a key role in the neurotoxicity of beta-amyloid: implications for Alzheimer's disease. *Aging Cell* **10**, 595–603.
- Zakharov SD, Hulleman JD, Dutseva EA, Antonenko YN, Rochet JC & Cramer WA (2007) Helical alpha-synuclein forms highly conductive ion channels. *Biochemistry* **46**, 14369–14379.
- Angelova PR, Ludtmann MH, Horrocks MH, Negoda A, Cremades N, Klenerman D, Dobson CM, Wood NW, Pavlov EV, Gandhi S *et al.* (2016) Ca²⁺ is a key

- factor in alpha-synuclein-induced neurotoxicity. *J Cell Sci* **129**, 1792–1801.
- 15 Patel N, Ramachandran S, Azimov R, Kagan BL & Lal R (2015) Ion channel formation by tau protein: implications for Alzheimer's disease and tauopathies. *Biochemistry* **54**, 7320–7325.
 - 16 Flach K, Hilbrich I, Schiffmann A, Gartner U, Kruger M, Leonhardt M, Waschipky H, Wick L, Arendt T & Holzer M (2012) Tau oligomers impair artificial membrane integrity and cellular viability. *J Biol Chem* **287**, 43223–43233.
 - 17 Kundel F, De S, Flagmeier P, Horrocks MH, Kjaergaard M, Shammas SL, Jackson SE, Dobson CM & Klenerman D (2018) Hsp70 inhibits the nucleation and elongation of tau and sequesters tau aggregates with high affinity. *ACS Chem Biol* **13**, 636–646.
 - 18 Kundel F, Hong L, Falcon B, McEwan WA, Michaels TCT, Meisl G, Esteras N, Abramov AY, Knowles TJP, Goedert M *et al.* (2018) Measurement of tau filament fragmentation provides insights into prion-like spreading. *ACS Chem Neurosci* **9**, 1276–1282.
 - 19 Abramov AY, Jacobson J, Wientjes F, Hothersall J, Canevari L & Duchen MR (2005) Expression and modulation of an NADPH oxidase in mammalian astrocytes. *J Neurosci* **25**, 9176–9184.
 - 20 Falcon B, Cavallini A, Angers R, Glover S, Murray TK, Barnham L, Jackson S, O'Neill MJ, Isaacs AM, Hutton ML *et al.* (2015) Conformation determines the seeding potencies of native and recombinant Tau aggregates. *J Biol Chem* **290**, 1049–1065.
 - 21 Zhang W, Falcon B, Murzin AG, Fan J, Crowther RA, Goedert M & Scheres SH (2019) Heparin-induced tau filaments are polymorphic and differ from those in Alzheimer's and Pick's diseases. *Elife* **8**, e43584.
 - 22 Narayan P, Holmstrom KM, Kim DH, Whitcomb DJ, Wilson MR, St George-Hyslop P, Wood NW, Dobson CM, Cho K, Abramov AY *et al.* (2014) Rare individual amyloid-beta oligomers act on astrocytes to initiate neuronal damage. *Biochemistry* **53**, 2442–2453.
 - 23 Pickhardt M, Lawatscheck C, Borner HG & Mandelkow E (2017) Inhibition of tau protein aggregation by rhodanine-based compounds solubilized via specific formulation additives to improve bioavailability and cell viability. *Curr Alzheimer Res* **14**, 742–752.
 - 24 David DC, Hauptmann S, Scherping I, Schuessel K, Keil U, Rizzu P, Ravid R, Drose S, Brandt U, Muller WE *et al.* (2005) Proteomic and functional analyses reveal a mitochondrial dysfunction in P301L tau transgenic mice. *J Biol Chem* **280**, 23802–23814.
 - 25 Britti E, Ros J, Esteras N & Abramov AY (2020) Tau inhibits mitochondrial calcium efflux and makes neurons vulnerable to calcium-induced cell death. *Cell Calcium* **86**, 102150.
 - 26 Vaarmann A, Gandhi S, Gourine AV & Abramov AY (2010) Novel pathway for an old neurotransmitter: dopamine-induced neuronal calcium signalling via receptor-independent mechanisms. *Cell Calcium* **48**, 176–182.